Materials Science in Semiconductor Processing 108 (2020) 104868

Contents lists available at ScienceDirect

Materials Science in Semiconductor Processing

journal homepage: http://www.elsevier.com/locate/mssp

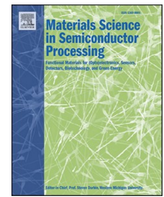

Effect of relative tool sharpness on subsurface damage and material recovery in nanometric cutting of mono-crystalline silicon: A molecular dynamics approach

Seyed Nader Ameli Kalkhoran [a,b], Mehrdad Vahdati [a,*], Jiwang Yan [b]

[a] Department of Mechanical Engineering, K.N. Toosi University of Technology, Pardis St, Vanak Sq, Tehran, Iran
[b] Department of Mechanical Engineering, Keio University, Hiyoshi 3-14-1, Kohoku-ku, Yokohama, 223-8522, Japan

ARTICLE INFO

Keywords:
Nanometric cutting
Molecular dynamics
Relative tool sharpness
Subsurface damage
Material recovery
Mono-crystalline silicon

ABSTRACT

Depth of cut (h_0) and tool edge radius (r_e) are two key parameters in nanometric cutting, investigating both of the two parameters simultaneously can provide comprehensive understanding of the cutting mechanism. In this paper, relative tool sharpness (RTS), which is quantified as h_0/r_e, is employed as a factor to examine the subsurface damage and material recovery in nanometric cutting of mono-crystalline silicon using molecular dynamics (MD) simulation. Various RTS values were generated by changes of cutting depth at different tool edge radius of 1, 3 and 5 nm respectively. Results indicate that there is always a layer of particles which sticks on the tool surface and influences the machined surface, even at RTS = 0. Besides that, the increase of RTS results in subsurface damage layer serration, which is caused by stick-slip phenomenon between the tool and workpiece. A bigger RTS causes a bigger depth of serrations, although the number of serrations remains constant. Increase in RTS also causes the formation of the hexagonal diamond structure. The material recovery drops dramatically by RTS increase. Using a sharper tool edge (RTS<0.25) at a cutting depths below 1 nm does not necessarily decrease subsurface damage due to the drastic stress concentration. It is also demonstrated that silicon amorphisation can occur in the unmachined region in front of the tool due to the hydrostatic pressure wave caused by tool advancement.

1. Introduction

Mono-crystalline silicon is an important engineering material which is widely used in optics, MEMS, electronics and solar cell industries due to its outstanding optical/electronic characteristics [1–3]. Nanometric cutting is one of the most effective ways to produce high precision optical silicon parts with mirror-like surface finish. In this method, the size scale of removed material is extremely small and comparable with the tool tip radius. Thus, both the undeformed chip thickness (UCT) and tool edge radius can affect the cutting mechanism including chip formation [4], heat generation [5], subsurface damages [6], material swelling [7], and tool wear [8].

Heat generation in the workpiece is due to various factors such as friction, kinetic energy changes and releasing the latent heat due to phase transformation [9]. MD simulation indicated that high temperature along with high pressure may lead to silicon carbide formation on the diamond tool contact area which reduces machined surface quality and tool life [10]. Subsurface damage is a critical aspect to consider when evaluating the quality of the ultimate machined surface. Phase transformation affects the hardness of workpiece surface and subsequent cutting paths [11]. It also affects the material side flow, cutting forces and workpiece temperature [12].

Surface generation mechanism in nanometric cutting is rather complicated and associated with the phenomena such as burnishing [5], elastic recovery [7,13] as well as material swelling and recovery [14, 15]. Fig. 1 shows the schematic diagram of different surface deformation during the nanometric cutting. Elastic recovery takes place on the tool-edge cut surface, due to material springs back elastically when the load is released. The amount of recovery depends on the cutting force and Young modulus of the subsurface material [14]. Besides, the material swelling occurs on the tool-nose cut surface. This is due to high pressure concentration beneath the cutting edge which push the material to the free surface [7]. Generally, there are two kinds of material swelling: side swelling and deep swelling [7,16]. Side swelling takes

* Corresponding author. Department of Mechanical Engineering, K.N. Toosi University of Technology, Pardis St, Vanak Sq, Tehran, Iran.
E-mail address: vahdati@kntu.ac.ir (M. Vahdati).

https://doi.org/10.1016/j.mssp.2019.104868
Received 25 August 2019; Received in revised form 1 November 2019; Accepted 26 November 2019
1369-8001/© 2019 Elsevier Ltd. All rights reserved.

Downloaded from Yan Laboratory, Keio University at http://www.yan.mech.keio.ac.jp. Redistribution is subject to copyright licence from the journal publisher.

place as a result of plastic side flow under high pressure. In such a case, the material flows toward the two sides of the cutting edge. However, deep swelling is the expansion of material volume at the bottom of the cutting edge, due to the thrust force. In current simulations, due to the full coverage of the workpiece width by the tool, there is no side swelling and only deep swelling will appear. Under this condition, the deep swelling can be considered as a subset of material recovery [14,17,18]. The effect of some parameters such as clearance angle [14] and workpiece temperature [15] on the material recovery behavior of metallic workpieces such as aluminum [7,14] and copper [7,17] have been extensively investigated. Nevertheless, the literature on material recovery in silicon cutting is very little.

In practice, depth of cut (h_0) and tool edge radius (r_e) are two main parameters which have significant impacts on characteristics of the machined parts. Relative tool sharpness (RTS), defined as h_0/r_e, is a useful parameter that encompasses both of these factors simultaneously. The RTS ratio can directly affect the machining quality, cutting temperature, subsurface damages as well as material recovery.

To understand the nanoscale cutting behavior, such as material recovery, that is difficult to realize by experiments, atomic scale simulations are necessary. Molecular Dynamics (MD) simulation is a powerful method which is able to provide an atomic vision to nanoscale material removal behaviors such as temperature variation, phase transformation, and material deformation. Arefin et al. [19] used 3 different cutting edge radii, 2.5, 4.0, and 6.0 nm and changed the depth of cut to keep the RTS equal to 0.8. They claimed that cutting edge radius has no obvious effect on the normal stresses σ_{xx} and σ_{yy}; though other RTS ratios were not studied. Zhang et al. [20] used an AFM-based diamond tool with the edge radius of 0.713 nm to investigate the effect of uncut chip thickness on the depth of subsurface deformed layer. They clarified that increasing the depth of cut to 0.5415 nm results in reaching the effective rake angle to the nominal rake angle and afterwards, there is no change in the depth of subsurface damaged layer. Zong et al. [17] exhibited that when RTS ratio is less than 1, material swelling and consequently surface roughness increase and the ploughing and burnishing phenomena take place. Zarechavoshi et al. [15] indicated that the amount of springback and thereby the elastic recovery is minor at the higher temperatures. However, the effect of tool edge radius and depth of cut were not considered. Wang et al. [21] used 5 different layered structure models which were a mixture of mono-crystalline and amorphous silicon. MD simulations were performed by a 5 nm edge radius diamond tool in the cutting depth of 5 nm ($h/r = 1$). Although springback and serrated subsurface damage occurred in the all conditions, these amounts were lower in the parts with an amorphous layer.

The effect of cutting parameters on subsurface damage has been considered by other researchers. Zhao et al. [22] used 3 different edge radii of 0, 3, and 5 nm and exposed that nanometric cutting causes β-silicon structure mixed with the amorphous phase. Moreover, it was illustrated that the thickness of amorphous phase layers rises by increasing the tool edge radius. Zhang et al. [23] clarified that by using a spherical diamond tool and increasing the cutting depth, the depth of subsurface damage increased dramatically. Lastly, they recommended the lower depth of cut should be chosen to achieve the minor subsurface damage. Dai et al. [24] used MD simulation to investigate the effect of tool geometry. They remarked that smaller edge radius tip would result in a smaller cutting force and a better subsurface. In another work by Dai et al. [25], a single-crystal silicon was machined by a structured diamond tool and it was elucidated that this tool causes the lower temperature increase, but more β-silicon phase. They also investigated the effect of cone-shaped tools with different tip angles in the cutting depth of 1 nm [26]. It was pointed out that the bigger apex angle results in higher transformed particles and the more extensive contact area should be the main reason for this. Recently, Liu et al. [27] revealed that the less amorphous structure phase transformation and the thinner subsurface damage layer occurs in the poly-crystalline silicon carbide because of material softening caused by the microstructure.

The previous researches are helpful in understanding the effect of tool edge radius and depth of cut on workpiece temperature and produced subsurface damages. Nevertheless, the impact of these two parameters has been considered separately, and up to date their relationship has not been clarified. To bridge the gap, the ratio of depth of cut (h_0) to tool edge radius (r_e) has been recently used for analyzing metal cutting process [28,29]; which is known as relative tool sharpness, RTS (h/r). The effect of this parameter on the cutting mechanisms and forces was already carried out by the present authors [30]. Likewise, it is expected that the investigation of the effects of RTS in silicon cutting enables to provide new findings on subsurface damage formation and material recovery. In this study, 6 different RTS values in 3 different tool edge radii were employed to understand the influence of this parameter and cutting mechanisms on workpiece temperature, subsurface damage, and material recovery. The effect of tool advancement on the creation of superficial damages over the unmachined surface was also investigated for the first time. Moreover, the evolution of amorphous layer as well as processing-induced phase transformation were investigated.

2. Molecular dynamics simulation details

2.1. Nanometric cutting model

The MD simulations were done by a computer code, known as “large-

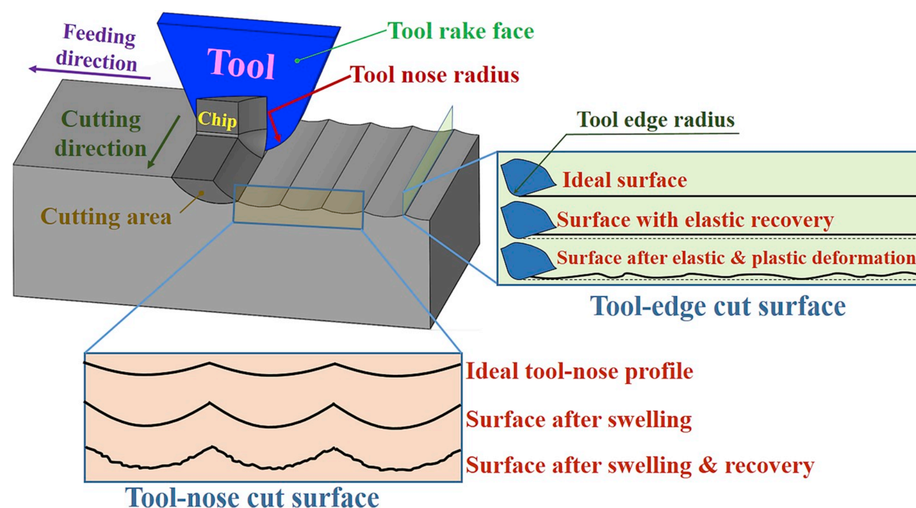

Fig. 1. The effect of material swelling and elastic recovery on nanometric cutting.

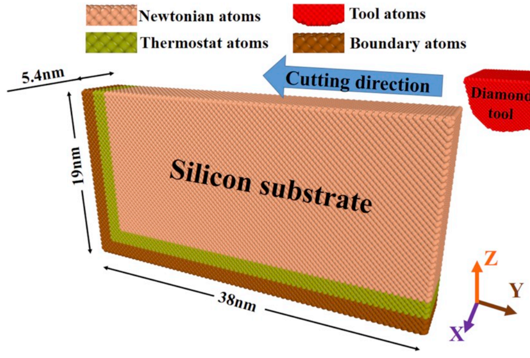

Fig. 2. 3D molecular dynamics model for nanometric cutting.

scale atomic/molecular massively parallel simulator" (LAMMPS) [31]. All the geometry and problem conditions were done by coding in this environment as follows.

The MD simulation model of the mono-crystal silicon with the initial temperature of 293K is shown in Fig. 2. The workpiece has a diamond cubic lattice structure without any defects. The dimensions of the workpiece are selected based on the recent research of the current authors [32]. This is the optimal size with the reasonable computational cost which is not affected by the workpiece size effect (such as initial shock or temperature fluctuations). It is comprised of three different kinds of atoms: boundary atoms, thermostat atoms, and Newtonian atoms. The left and bottom side atoms are kept fixed in three layers to prevent workpiece movement during the simulation. The three layers above the boundary atom layers are thermostat atoms of which the temperature is kept at 293K (equal to the initial temperature of the workpiece) using the velocity rescaling method, at every 10 computational time steps, to imitate the heat dissipation [33]. This is a common method for keeping the temperature of this area constant which has been used by many scholars [34–36]. The rest of the workpiece particles (pink colored atoms) are the Newtonian atoms, which are in the main area in this investigation. The motions of the thermostat and Newtonian atoms obey the classical second Newton's law. In order to eliminate the boundary effects, the periodic boundary condition is applied to the x direction. Owing to the high resistance of the single-crystal diamond tool, it is considered as a rigid body; with the rake angle and clearance angle of −10 and 15°, respectively.

Six different RTS values is studied as 0, 0.1, 0.25, 0.5, 0.75 and 1. These values are not only defined by changing the depth of cut, nor tool edge radius; But by changing both of these parameters simultaneously. In this arrangement, we could investigate the effect of RTS more comprehensively. All the cutting simulations are conducted on the (001) plane in the $[0\,\bar{1}\,0]$ direction with a cutting distance of 20 nm. Also, the cutting velocity of 100 m/s is used in this work.

2.2. Interatomic potentials

Choosing the appropriate potential function for defining the interaction of different atoms is the most important step in a MD simulation. In this research, the semi-empirical and three-body Tersoff empirical potential function is employed to describe the interaction between Si–Si and Si–C atoms [60]. This is a well-known and powerful potential function which successfully describes the properties and structure of the covalently bounded systems such as silicon [25,37,38]. The interatomic potential is expressed as follows [39,40]:

$$E = \sum_i E_i = \frac{1}{2}\sum_i \sum_{j\neq i} U(r_{ij}) \tag{1}$$

$$U(r_{ij}) = f_c(r_{ij})\left[a_{ij} f_R(r_{ij}) + b_{ij} f_A(r_{ij})\right] \tag{2}$$

where E is the total energy of the system, which is decomposed for convenience into a site energy E_i and a bond energy $U(r_{ij})$. In here, f_R is the 2-body term and f_A includes 3-body interactions, are taken to be:

$$f_R(r) = A\,\exp(-\lambda_1 r), \tag{3}$$

$$f_A(r) = -B\,\exp(-\lambda_2 r), \tag{4}$$

$$f_c(r) = \begin{cases} 1, & r < R - D \\ \frac{1}{2} - \frac{1}{2}\sin\left[\frac{\frac{\pi}{2}(r-R)}{D}\right], & R - D < r < R + D \\ 0, & r > R + D \end{cases} \tag{5}$$

$$b_{ij} = \left(1 + \beta^n \zeta_{ij}^n\right)^{-1/2n}, \tag{6}$$

$$\zeta_{ij}^n = \sum_{k(\neq i,j)} f_c(r_{ik}) g(\theta_{ijk}), \tag{7}$$

$$g(\theta) = 1 + \frac{c^2}{d^2} - \frac{c^2}{\left[d^2 + (h - \cos\theta)^2\right]}, \tag{8}$$

$$a_{ij} = \left(1 + \alpha^n \eta_{ij}^n\right)^{-1/2n}, \tag{9}$$

$$\eta_{ij} = \sum_{k(\neq i,j)} f_c(r_{ik}) \exp\left[\lambda_3^3 (r_{ij} - r_{ik})^3\right] \tag{10}$$

The constant values of these equations are depending on the materials as well as the modifications have been applied to them during the years. The parameters used in the current work are listed in Table 1. Furthermore, the C–C interaction of the diamond tool is ignored because of the rigid body attribute.

Table 1
Parameters of the Tersoff potential function used in this paper [31,41].

Parameters	Si–Si–Si	Si–Si–C	Si–C–C	C–Si–Si	C–Si–C	C–C–Si	Si–C–Si
A (eV)	1830.8	0	1597.3111	1597.3111	0	0	0
B (eV)	471.18	0	395.126	395.126	0	0	0
D (Å)	0.15	0.15	0.15	0.15	0.15	0.15	0.15
R (Å)	2.85	2.36	2.36	2.36	1.95	2.36	2.85
λ_1 (Å $^{-1}$)	2.4799	0	2.9839	2.9839	0	0	0
λ_2 (Å $^{-1}$)	1.73222	0	1.97205	1.97205	0	0	0
β	0.0000011	0	0.0000011	0.00000015724	0	0	0
n	0.78734	0	0.787340	0.72751	0	0	0
c	100390	100390	100390	38049	38049	38049	100390
d	16.217	16.217	16.217	4.3484	4.3484	4.3484	16.217
h	−0.59825	−0.59825	−0.59825	−0.57058	−0.57058	−0.57058	−0.59825

Table 2
Computational parameters employed in the MD simulations.

Cutting parameters	Value
Workpiece	Mono-crystalline silicon
Number of workpiece atoms	198110
Initial temperature	293K
Interatomic interaction	Tersoff (Si–Si, Si–C)
Number of fixed layers/atoms	3/26590
Number of thermostatic layers/atoms	3/25030
Uncut chip thickness (Depth of cut in 2D)	0–5 nm
Tool	Rigid diamond
Tool edge radius	1, 3, 5 nm
Rake angle	−10
Clearance angle	15
Cutting speed	100 m/s
RTS	0, 0.1, 0.25, 0.5, 0.75, 1
Cutting distance	20 nm
Cutting plane and cutting orientation	(001)[0 $\bar{1}$ 0]
Time step	1 fs

2.3. Simulation procedure

Before beginning the cutting process, the model is optimized using two stages of minimization and one equilibrium step. The first minimization is performed just after the definition of the workpiece and tool.

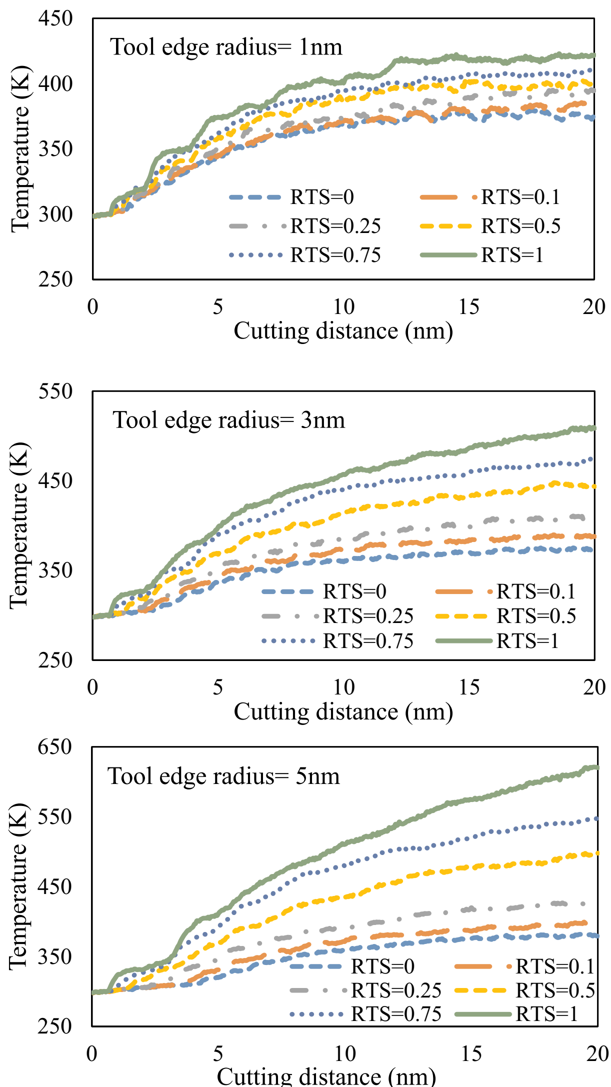

Fig. 3. Workpiece temperature rise during the cutting.

Afterwards, the tool is moved to the desired depth of cut and the second minimization is applied. Finally, the system is left for 25 ps for the perfect equilibration. The NVT canonical ensemble (constant atom number N, constant volume V and constant temperature T) was used in the equilibration stage. The constant temperature during this stage was defined as the initial temperature of the workpiece (293K). In this circumstance, the system finds its equilibrium state, while keeping the workpiece temperature as the initial value.

Then, the main MD calculations (cutting process) were performed under a microcanonical (NVE) ensemble. Moreover, the equations of motion were integrated using the velocity-Verlet algorithm with the time steps of 1 fs. In order to visualize and post-process of the simulations, Open Visualization Tool (OVITO) [42] is used. The simulations were run on a high-performance computer with the total of 48 cores at Yan laboratory, Keio University. The computation time for each simulation was between a few hours to 3 days. The details and parameters of the simulations are summarized in Table 2.

3. Results and discussion

3.1. Cutting temperature

Typically, the temperature is influenced by the energy input, which is directly related to the material removal rate. So, it would be affected under different RTS ratios. Fig. 3 presents the temperature variation of the workpiece during the cutting process at different RTS values and tool edge radii. Although the temperature is calculated for the mobile atoms (Newtonian atoms + Thermostat atoms), it is mostly (84.5%) dependent on the Newtonian region. It can be seen that increase in both RTS and tool edge radius results in the increase of the workpiece temperature. The explanation for this is the presence of more atoms in front of the tool and, consequently, more increase in the kinetic energy of the system due to the higher movement of the particles. Since kinetic energy and temperature of the system are in direct relationship with one another, this will eventually increase the temperature of the workpiece. Additionally, defect accumulation and, as a result, stress concentration are another reasons for temperature increase by tool advancement. These issues lead to thermal softening and reduce the friction coefficient [43]. Friction coefficient is defined as the ratio of tangential force to thrust force and is reversely proportional to the force angle [44]. Thus, the reason for the increase of force angle (decrease in friction coefficient) at the greater RTS values, in the previous research [30], can be explained. It can also be observed that at the minor RTS values where rubbing and ploughing mechanisms are dominant and there is no chip formation, the workpiece temperature still increases. This is mostly owing to friction, and not the variation of kinetic energy.

Fig. 3.a indicates severe temperature fluctuations at RTS = 0. In this

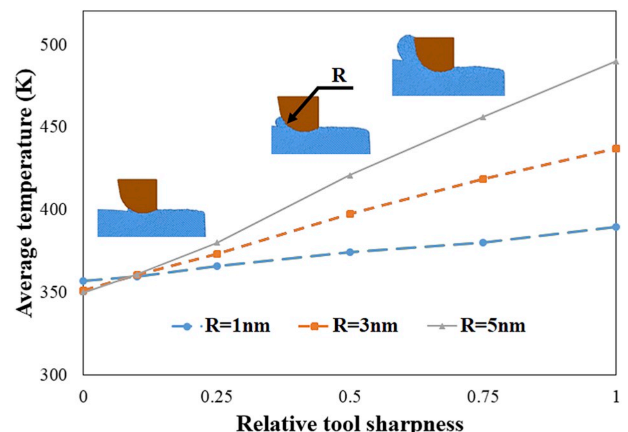

Fig. 4. Average temperature during nanometric cutting.

circumstance, friction and particles movement increase the workpiece temperature. On the other hand, some of the atoms, which their atomic bonds have been already broken due to the severe kinetic energy changes, have the chance to make a covalent bonding; and this will be along with temperature decreasing. The effect of this fluctuation is even seen at the higher RTS value. These instabilities can affect brittle materials such as silicon. Hence, in spite of the common belief, reducing the tool edge radius will not necessarily result in the better machined surface.

Fig. 3 also highlights that the increasing trend has been decreased after a certain tool advancement, especially at the lower RTS values. In this distance, the tool fully entered into the workpiece and the number of atoms ahead and behind it are stable. Therefore, it could be claimed that the number of defects has reached to the critical level and no significant change will occur with the further tool advancement. Dai et al. [25] used 4 types of tool patterns in their research and also found that the cutting temperature reached its maximum value after 11 nm tool advancement. Likewise, in a study by Goel et al. [45] using a cutting edge radius of 1.322 nm in the cutting depth of 1.322 (RTS = 1), the cutting temperature reached 460 °C after 20 nm tool movement. Although the rake and clearance angle used in their research were quite different from the present work, this temperature is within our range.

To determine the effect of RTS value as well as tool edge radius on workpiece temperature, the average temperature evolution was plotted, as shown in Fig. 4. According to this figure, the temperature almost increases linearly by increasing the relative tool sharpness. Increasing in the tool edge radius, changes the volume of removed material and hence, the trend of variation gets sharper. The slope of these changes for tools with the edge radius of 1, 3 and 5 nm is 32.71, 86.37 and 140.15, respectively. This figure also demonstrates that at RTS = 0, the sharper tool increases the workpiece temperature more than the other two tools. It is because the ploughing mechanism runs in this tool. That is while, the other tools are into the rubbing mechanism, which brings lower energy inside the workpiece.

Interestingly, the workpiece temperature is independent of the tool edge radius at RTS = 0.1. Since there is no efficient material removing in this condition, in cases that the surface quality is not crucial, it may be possible to use this method as a kind of heat treatment process.

3.2. Subsurface damage

Ductile mode machining does not necessarily mean a damage-free process. Thus, considerable subsurface damage (SSD) will occur to the substrate material. Fig. 5 displays material removal and evolution of subsurface damage induced by a 3-nm tool in a mono-crystalline silicon after 20 nm cutting distance and at different RTS ratios. This is provided by the Common Neighbor Analysis (CNA) [46,47]. Perfect cubic diamond structure (Si–I) is removed for better visualization. The gray particles present the amorphous structure. The depth of SSD is various along with the cutting surface. Hence, the average depth of SSD was defined and ImageJ software was used to measure its depth. The depth of SSD was measured in comparison to the tool dimension. Furthermore, the blue and green particles show the first and second neighbors of cubic diamond structure, respectively. The presence of these atoms on the workpiece surface and amorphous border indicates the border of crystalline structure (with dangling bonds); and also, their existence inside the workpiece shows body centered tetragonal (β–silicon) structure as well as the dislocations [27]. The phase transformation is partly due to chemical affinity between tool and workpiece and mostly because of hydrostatic stress. The threshold pressure for dislocation initiation for silicon is a little higher than the threshold pressure for amorphisation [48]. Therefore, by increasing the RTS to 0.25, the evolution of dislocations (blue particles) initiates from the bottom of the tool (Fig. 5c). They are mainly of screw dislocations, which form with a Burger's vector parallel to the dislocation line. However, there is no noticeable change in their number. So that, for the RTS ratios of 0.5, 0.75 and 1 the number of them are 7720, 7791 and 7734, respectively. These numbers are interestingly close to one another, with less than 1% difference.

Fig. 6.a1 and b1 show stress fields in the workpiece at different depth of cuts. As can be seen, the larger RTS ratio results in the bigger pressure zone. Fig. 6.a2 demonstrates the scheme of cutting condition at RTS = 0.25, which more fraction of the atoms in front of the tool is pressed downwards and causes the dislocations. Increasing RTS to 1 leads to reducing this fraction, and on the contrary, expanding the pressure zone in front of the tool (Fig. 6b). For this reason, there is a compromise between these two phenomena which retains the number and depth of dislocations constant. Yan et al. also found empirically that the depth of dislocations is not related to the cutting conditions [6].

An amorphous layer has been always created on the machined surface. Under high hydrostatic and shear stress conditions, a large number of pristine silicon atoms will be directly transformed into amorphous silicon (a-Si). However, it is observed that amorphous layer serration starts from RTS of 0.5. The depth of these serrations increases with the increase of RTS, so that it reaches to 4.43 nm at RTS = 1. This may be due to stick-slip phenomenon between the tool and workpiece. A great deal of researches has proved the existence of this phenomenon in nanometric cutting [49–51]. Its occurrence is positively correlated with the cutting forces, which was examined in the preceding research done by the present authors [30]. Therefore, it can be claimed that at this RTS, the cutting force has reached its critical level for the occurrence of stick-slip phenomenon.

By increasing RTS to 0.75, the hydrostatic pressure is increased and a few of particles beneath the machined surface transformed into the hexagonal diamond structure (the orange-color particles). This phase

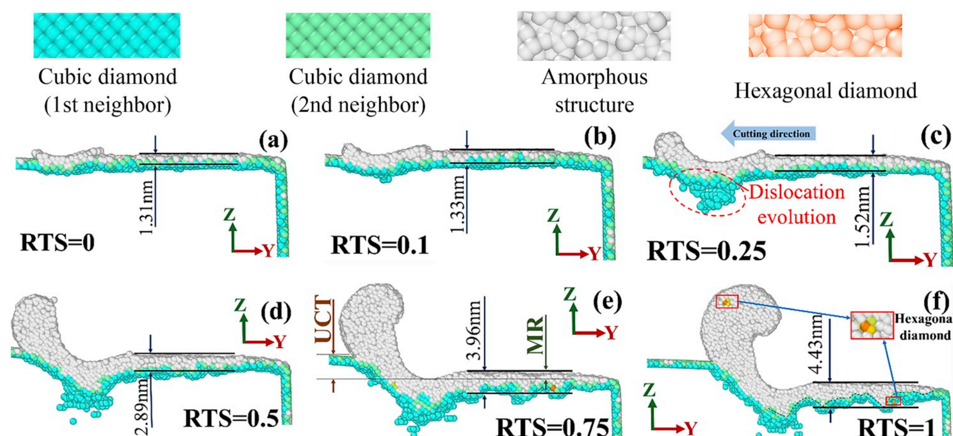

Fig. 5. Evolution snapshot of the different defects during the nanometric cutting at different RTS (R = 3 nm).

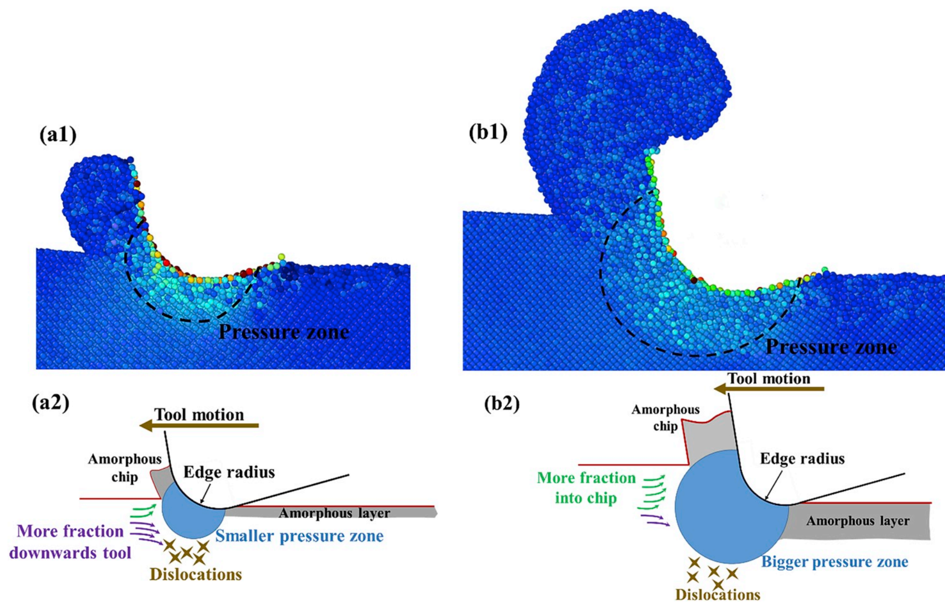

Fig. 6. Effect of RTS on stress field and creation of dislocations at (a) RTS = 0.25, and (b) RTS = 1 (R = 3 nm).

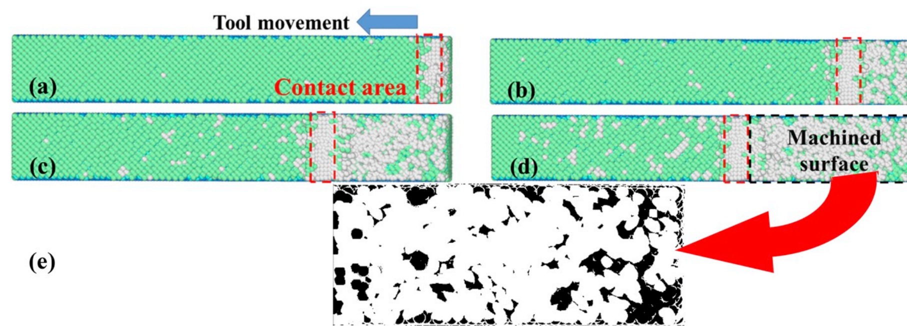

Fig. 7. Surface generation process from top view after (a) 5 nm, (b) 10 nm, (c) 15n, (d) 20 nm tool advancement and (e) image-processed result for calculation of machined surface amorphisation by ImageJ software.

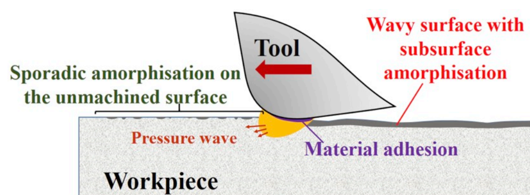

Fig. 8. Effect of adhered layer on amorphisation of unmachined surface.

transformation increases with increasing the relative tool sharpness, and even can be seen in the chip area. In all circumstances, no evidence of Si–I was found in the chip area. Therefore, it can be claimed that the ductile mode machining is predominant.

Machined surface amorphisation is observed even at RTS = 0, with the thickness of 1.31 nm (Fig. 5a). The top view of this situation during the different tool advancements is presented in Fig. 7 (the diamond tool is removed). Although the initial unmachined surface was totally in diamond structure, tool rubbing leads to a ragged surface with amorphisation. This is due to sticking an atomic layer on the tool edge and messing the surface atoms. Interestingly, there is no change in the freshly machined surface arrangement by tool movement. The result obtained from image processing of this surface by the ImageJ software shows 84% amorphisation in this area (Fig. 7e).

Conversely, the number of particles in amorphous structure is increasing on the unmachined region by tool advancement. According to Fig. 8, the stuck atomic layer on the tool edge enters a hydrostatic pressure wave into the workpiece. This issue results in impaction breaking in Si–Si bonds as well as increasing the potential energy in the primary shear zone. Subsequently, the workpiece's temperature and stress are changed and a fraction of unmachined surface atoms is converted to amorphous ones.

According to the physical analysis, reducing the cutting edge radius up to 1 nm, leads to variation in the energy balance between the substrate surface and elastic strain energies [13]. Hence, different behaviors are expected. The trend of subsurface damage evolution with a 1-nm tool edge radius at different RTS values is displayed in Fig. 9. By comparison these results with Fig. 5, it can be found that the depth of amorphisation at relative tool sharpness ratios of 1 and 0.1 is 5.03 and 1.83% further than the tool with the edge radius of 3 nm. It is likely due to the lower tool-workpiece contact surface in 1-nm tool edge which leads to the higher stress concentration on the tool tip area. However, the nucleation site of dislocations is still under the cutting edge curve due to the highest material deformation rate.

Besides that, the initiation of phase transformation to hexagonal diamond is again from RTS = 0.75. Though, all these phase transformations take place in the chip and no signs of them can be seen on the machined surface. Likewise, there is no hexagonal phase transformation even at RTS of unit. Due to this feature, it can be argued that the sharper

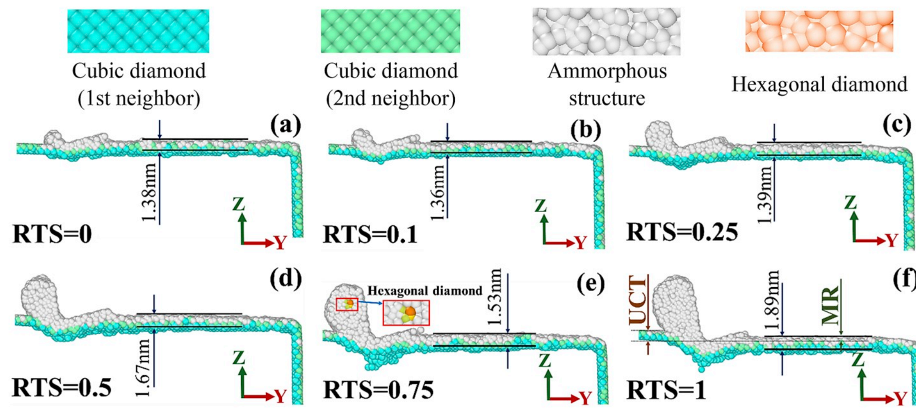

Fig. 9. Evolution snapshot of the different defects during the nanometric cutting at different RTS (R = 1 nm).

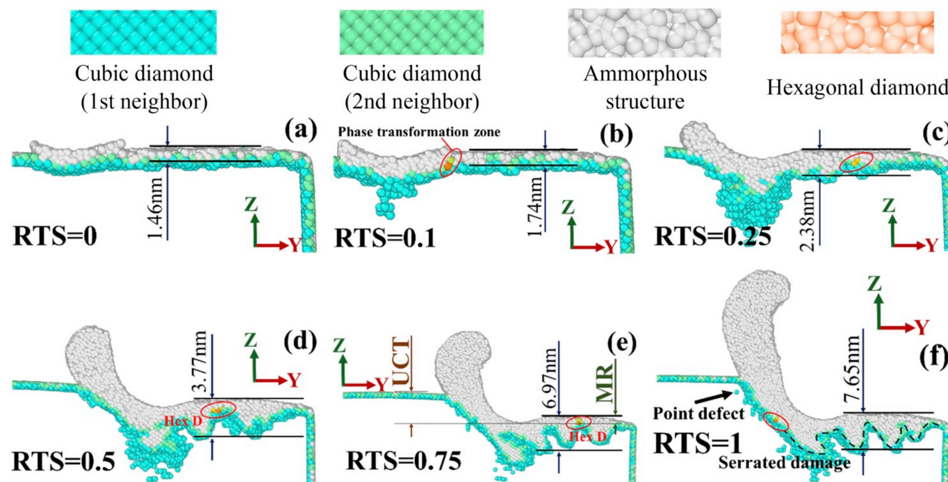

Fig. 10. Evolution snapshot of the different defects during the nanometric cutting at different RTS (R = 5 nm- Video is available in online format).

tool edge radius causes the lower phase transformation on the machined surface. Another attractive output is that there is no serrated subsurface damage beneath the machined area. The main reason for this is the minor depth of cut and consequently, the insignificant cutting forces [30]. Additionally, the depth of dislocations is much lower in the sharper tool edge and at the same RTS.

The depth of SSD reaches 7.65 nm at RTS = 1. In a research conducted by Wang et al. [21], the depth of SSD was reported to be 3.8 nm; which is about half of the value obtained in the present work. This is due to the double cutting speed (200 m/s) in their study. According to the previous researches, the higher cutting speed will result in lower subsurface damage [52].

The evolution of subsurface damages at different RTS and for the 5-nm tool is shown in Fig. 10. Although the general chip formation and amorphisation are similar to the tool with the edge radius of 3 nm, a few distinctions can be seen. In this tool, the depth of amorphous structure is always higher than that of two sharper tools. Besides, due to the higher hydrostatic pressure, hexagonal phase transformation appears sooner and at the RTS of 0.1.

In such a way, by increasing RTS to 0.25, the serrated subsurface damage initiates. Although the depth of these serrations increases up to 3.3 times by increasing RTS, appealingly, the number of them has remained the same and equals to 4. As it was mentioned, subsurface serration is owing to slip-stick. The creation of slip-stick phenomenon depends on cutting speed and material stiffness [53]. Given the fact that these two parameters are constant at different RTS values, it can be concluded that the number of them should be the same. In the

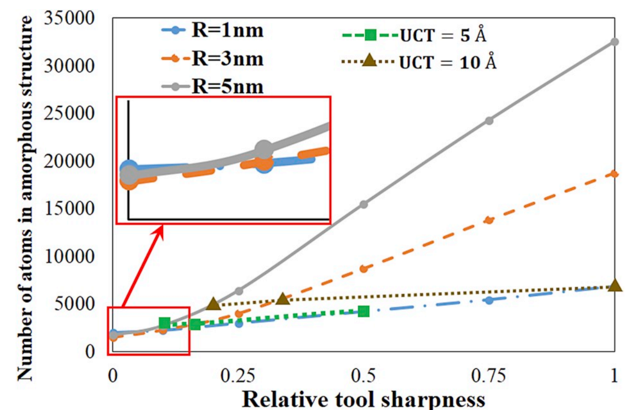

Fig. 11. Variation of atoms in the amorphous structure.

meantime, the edges of these serrations are roughly at an angle of 45. This occurred because of silicon structure slipping along cleavage planes {111}. Typically, the growth of plastic deformation on the cleavage planes needs the lowest energy [54].

For this edge radius, the highest depth of SSD occurs at RTS = 1 which is 4.43 nm. This value was 2.1 nm is a study by Zhang et al. [23]. However, they used a cylindrical cutting tool with the cutting speed of 160 m/s.

Moreover, in spite of 2 sharper tools, there are a few point defects in

front of the tool and at the higher RTS values. Here, the point defects specifically refer to "self-interstitial atoms"; which are the extra atoms which have embedded into an interstitial void inside the crystal structure. They are due to the larger plastic deformation which takes place in this circumstance and increases the hydrostatic pressure in the primary shear zone. However, the cutting mechanism is still as plastic flow and no transgranular fracture occurred. Besides, there are no fractures and cracks on the freshly machined surface. The main reason for this issue is filling cavities by the ductile metallic silicon phase which is later transformed to amorphous phase [55]. The video of Fig. 10.f, which is available in the online version, demonstrates this issue.

The influence of different tool edge radii and RTS values on the number of atoms in the amorphous area is plotted in Fig. 11. This kind of atoms increases quasi-linearly with increasing the RTS. Since the amorphisation and temperature increase are directly proportional to one another [43], there was a similar trend in temperature variation with the increase in RTS (Fig. 4). Further, the cutting forces go up with the augmentation of the RTS [30]. This accelerates the nucleation of dislocations and their movement [35]. Accordingly, the process enters into a situation which results in increasing in the workpiece temperature and meanwhile, the subsurface damage.

As shown earlier, even at the RTS of 0, a number of surface atoms are transformed to the amorphous structure. However, the number of these atoms in the tool with an edge radius of 1 nm is about 13.4 and 22.8% bigger than those in the other two tools. This is due to the ploughing mechanism which occurs earlier in the sharper tool and results in the higher distortion. At the higher RTS values, the chip formation mechanism enters into the shearing and the blunter tool causes more amorphous structure. For instance, in the case of RTS = 1, the number of atoms in amorphous structure which are created by the 5-nm tool, are 1.73 and 4.78 times bigger than those of the tools with the edge radius of 3 and 1 nm, respectively. Nevertheless, it should be noted that in this condition, the depth of cut is higher too. Hence, in order to a better comparison, the trend of amorphisation is added in two cutting depths of 5 and 10 Å. Surprisingly, the number of amorphous atoms in the 5-nm tool, is always smaller than those of two sharper tools. But this does not necessarily mean fewer damages on the machined surface, because a significant percentage of amorphous atoms is always located in the chip area.

For this reason, the effect of RTS on the depth of subsurface damage is plotted in Fig. 12. It is seen that the depth of amorphisation is almost independent of the RTS in the 1-nm tool. In here, the depth of cut is always less than 1 nm and thus, the pressure zone beneath the tool is not significant. On the other hand, due to the minor cutting depth, the particles ahead of the tool are transmitted faster to behind the tool and as a result, they are less affected by the tool pressure. Eventually, these issues cause no significant change in the quality of the machined surface.

It is also screened that the depth of SSD increases by increasing the tool edge radius at a constant RTS. However, the depths of amorphisation in the two cutting depths of 5 and 10 Å provide new results. The results exhibit that the minimum SSD at the cutting depth of 5 Å is obtained using a tool with the edge radius of 3 nm. In this cutting depth, the 5-nm tool edge is still under the influence of the ploughing mechanism, and so the atomic messing beneath the tool is large. Besides, immense stress concentration always comes along with the 1-nm tool. Thus, this ultra-sharp tool could affect the machined surface badly at the lower depths of cut.

Increasing the cutting depth to 1 nm, corroborates the literature about using the sharper tool edge in achieving the lower SSD [56,57]. The reason for this is the more contact surface at the bigger tool edge radius; and accordingly, the higher material deformation and hydrostatic pressures [26]. Therefore, it can be claimed generally that in the condition which the RTS is more than 0.25 and the depth of cut is upper than 1 nm, utilization of the sharper tool edge leads to the lower amorphisation and the thinner SSD.

3.3. Material recovery

In order to investigate the material recovery (MR) and swelling, the following definition is used:

$$MR\% = h_s/h_i \times 100 \quad (11)$$

In which h_s is the height of surface swelling and h_i is the ideal depth of cut.

Fig. 13 presents the variation of MR at the different tool edge radii and RTS values. This plot demonstrates that increasing RTS always results in reducing the MR. The amount of elastic recovery depends on the material properties (hardness and elastic modulus) as well as tool geometry [17,58]. Hence, by reducing the cutting depth in a specific tool edge radius (reducing the RTS value), the same springback force enters into the smaller cutting area. Therefore, the specific cutting energy is greatly increased and as a consequence, the material recovery ascends.

Furthermore, the heat generation during the nanometric cutting can influence the MR [59]. As observed in Fig. 4, the workpiece temperature rises by increasing the RTS value. This evolution leads to reducing of spring back and elastic recovery in the workpiece [15]. Hence, this is another reason for MR reduction at the higher RTS values.

4. Conclusions

This paper investigates the influence of relative tool sharpness (RTS) on temperature, subsurface damage, and material recovery in nanometric cutting of the mono-crystalline silicon. The main results are summarized below:

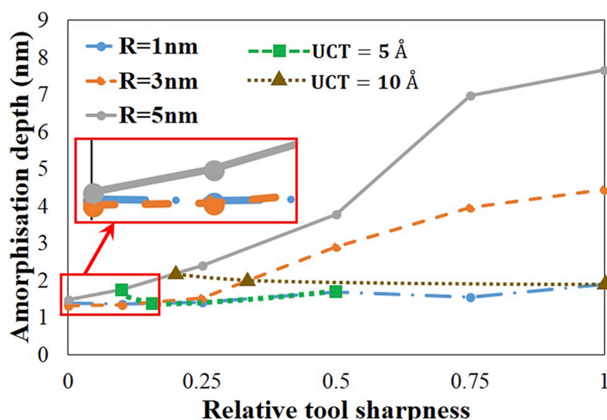

Fig. 12. The effect of RTS on the depth of subsurface damage.

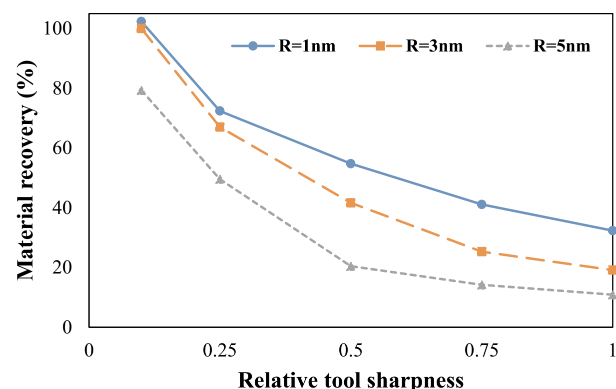

Fig. 13. Effect of RTS on material recovery.

- Increase tool edge radius and RTS results in lower material recovery and higher temperature of the cutting region. The temperature is independent of tool edge radius at RTS of 0.25.
- With the increase of the RTS, dislocations initiate from beneath of the tool; but there is no significant change in the number and depth of the dislocation. Increase in RTS also causes formation of the hexagonal diamond structure.
- Regardless of the RTS ratio, a layer of silicon atoms always adheres on the tool surface and affects the surface integrity. It can even influence the unmachined surface quality.
- An amorphous layer is always created on the machined surface. Increasing depth of cut leads to the serration of the amorphous layer. Although the depth of serrations increases greatly by increasing RTS, the number of them remains the same.
- Amorphisation takes place in a small regions in the unmachined region in front of the tool. With tool advancement, point defects are also generated in front of the tool.
- At an extremely small tool edge radius (1 nm) and RTS (0), temperature fluctuations occur. The depth of machining-induced amorphous layer is independent of RTS, and the serration of the amorphous layer does not appear.

This study demonstrated the importance of relative tool sharpness in nanometric cutting and identified the critical RTS which affects the cutting mechanism and the surface integrity. These findings could help to choose the better parameters for machining of mono-crystal silicon.

Declaration of competing interest

The authors declare that they have no known competing financial interests or personal relationships that could have appeared to influence the work reported in this paper.

Appendix A. Supplementary data

Supplementary data to this article can be found online at https://doi.org/10.1016/j.mssp.2019.104868.

References

[1] J. Yan, M. Yoshino, T. Kuriagawa, T. Shirakashi, K. Syoji, R. Komanduri, On the ductile machining of silicon for micro electro-mechanical systems (MEMS), opto-electronic and optical applications, Mater. Sci. Eng. A 297 (2001) 230–234, https://doi.org/10.1016/S0921-5093(00)01031-5.

[2] B. Nunes, S. Magalhães, N. Franco, E. Alves, R. Colaço, Microstructure and nanomechanical properties of Fe+ implanted silicon, Appl. Surf. Sci. 284 (2013) 533–539, https://doi.org/10.1016/j.apsusc.2013.07.129.

[3] M. Heidari, J. Yan, Ultraprecision surface flattening of porous silicon by diamond turning, Precis. Eng. 49 (2017) 262–277, https://doi.org/10.1016/j.precisioneng.2017.02.015.

[4] J. Yan, K. Syoji, T. Kuriyagawa, H. Suzuki, Ductile regime turning at large tool feed, J. Mater. Process. Technol. 121 (2002) 363–372, https://doi.org/10.1016/S0924-0136(01)01218-3.

[5] J. Yan, H. Zhao, T. Kuriyagawa, Effects of tool edge radius on ductile machining of silicon: an investigation by FEM, Semicond. Sci. Technol. 24 (2009), 075018, https://doi.org/10.1088/0268-1242/24/7/075018.

[6] J. Yan, T. Asami, H. Harada, T. Kuriyagawa, Fundamental investigation of subsurface damage in single crystalline silicon caused by diamond machining, Precis. Eng. 33 (2009) 378–386, https://doi.org/10.1016/j.precisioneng.2008.10.008.

[7] S. To, C.F. Cheung, W.B. Lee, Influence of material swelling on surface roughness in diamond turning of single crystals, Mater. Sci. Technol. 17 (2001) 102–108, https://doi.org/10.1179/026708301101509025.

[8] J. Yan, K. Syoji, J. Tamaki, Some observations on the wear of diamond tools in ultra-precision cutting of single-crystal silicon, Wear 255 (2003) 1380–1387, https://doi.org/10.1016/S0043-1648(03)00076-0.

[9] L. Shi, J. Xie, M. Xi, X. Li, F. Yu, Study on cutting mechanism of monocrystalline silicon using molecular dynamics on nanometric scale, in: Int. Conf. Mater. Sci. Appl, ICMSA 2015, Suzhou, China, 2015, pp. 117–120.

[10] S. Goel, X. Luo, R.L. Reuben, Wear mechanism of diamond tools against single crystal silicon in single point diamond turning process, Tribol. Int. 57 (2013) 272–281, https://doi.org/10.1016/j.triboint.2012.06.027.

[11] J. Yan, H. Takahashi, J. Tamaki, X. Gai, T. Kuriyagawa, Transmission electron microscopic observation of nanoindentations made on ductile-machined silicon wafers, Appl. Phys. Lett. 87 (2005) 211901, https://doi.org/10.1063/1.2133908.

[12] F. Xu, F. Fang, X. Zhang, Effects of recovery and side flow on surface generation in nano-cutting of single crystal silicon, Comput. Mater. Sci. 143 (2018) 133–142, https://doi.org/10.1016/j.commatsci.2017.11.002.

[13] S.S. To, H. Wang, W.B. Lee, Materials Characterisation and Mechanism of Micro-cutting in Ultra-precision Diamond Turning, Springer Berlin Heidelberg, Berlin, Heidelberg, 2018, https://doi.org/10.1007/978-3-662-54823-3.

[14] M.C. Kong, W.B. Lee, C.F. Cheung, S. To, A study of materials swelling and recovery in single-point diamond turning of ductile materials, J. Mater. Process. Technol. 180 (2006) 210–215, https://doi.org/10.1016/j.jmatprotec.2006.06.006.

[15] S.Z. Chavoshi, S. Goel, X. Luo, Molecular dynamics simulation investigation on the plastic flow behaviour of silicon during nanometric cutting, Model. Simul. Mater. Sci. Eng. 24 (2016), 015002, https://doi.org/10.1088/0965-0393/24/1/015002.

[16] W.S. Yip, S. To, Reduction of material swelling and recovery of titanium alloys in diamond cutting by magnetic field assistance, J. Alloy. Comp. 722 (2017) 525–531, https://doi.org/10.1016/j.jallcom.2017.06.167.

[17] W.J.J. Zong, Y.H.H. Huang, Y.L.L. Zhang, T. Sun, Conservation law of surface roughness in single point diamond turning, Int. J. Mach. Tool Manuf. 84 (2014) 58–63, https://doi.org/10.1016/j.ijmachtools.2014.04.006.

[18] M. Tauhiduzzaman, S.C. Veldhuis, Effect of material microstructure and tool geometry on surface generation in single point diamond turning, Precis. Eng. 38 (2014) 481–491, https://doi.org/10.1016/j.precisioneng.2014.01.002.

[19] S. Arefin, X.P. Li, M.B. Cai, M. Rahman, K. Liu, A. Tay, The effect of the cutting edge radius on a machined surface in the nanoscale ductile mode cutting of silicon wafer, Proc. Inst. Mech. Eng. B J. Eng. Manuf. 221 (2007) 213–220, https://doi.org/10.1243/09544054JEM568.

[20] J.J. Zhang, T. Sun, Y.D. Yan, Y.C. Liang, S. Dong, Molecular dynamics simulation of subsurface deformed layers in AFM-based nanometric cutting process, Appl. Surf. Sci. 254 (2008) 4774–4779, https://doi.org/10.1016/j.apsusc.2008.01.096.

[21] J. Wang, F. Fang, X. Zhang, Nanometric cutting of silicon with an amorphous-crystalline layered structure: a molecular dynamics study, Nanoscale Res. Lett. 12 (2017) 41, https://doi.org/10.1186/s11671-017-1829-y.

[22] H. Zhao, C. Shi, P. Zhang, L. Zhang, H. Huang, J. Yan, Research on the effects of machining-induced subsurface damages on mono-crystalline silicon via molecular dynamics simulation, Appl. Surf. Sci. 259 (2012) 66–71, https://doi.org/10.1016/j.apsusc.2012.06.087.

[23] F.Q. Zhiwei Zhang, Pei Chen, Molecular dynamics simulation on subsurface damage layer during nano grinding process of silicon wafer, in: 18th Int. Conf. Electron. Packag, 2017, pp. 487–490.

[24] H. Dai, G. Chen, Q. Fang, J. Yin, The effect of tool geometry on subsurface damage and material removal in nanometric cutting single-crystal silicon by a molecular dynamics simulation, Appl. Phys. A 122 (2016) 804, https://doi.org/10.1007/s00339-016-0319-x.

[25] H. Dai, G. Chen, C. Zhou, Q. Fang, X. Fei, A numerical study of ultraprecision machining of monocrystalline silicon with laser nano-structured diamond tools by atomistic simulation, Appl. Surf. Sci. 393 (2017) 405–416, https://doi.org/10.1016/j.apsusc.2016.10.014.

[26] H. Dai, S. Li, G. Chen, Molecular dynamics simulation of subsurface damage mechanism during nanoscratching of single crystal silicon, Proc. Inst. Mech. Eng. J J. Eng. Tribol. 233 (2019) 61–73, https://doi.org/10.1177/1350650118765351.

[27] Y. Liu, B. Li, L. Kong, Molecular dynamics simulation of silicon carbide nanoscale material removal behavior, Ceram. Int. 44 (2018) 11910–11913, https://doi.org/10.1016/j.ceramint.2018.03.195.

[28] M.A. Rahman, M.R. Amrun, M. Rahman, A.S. Kumar, Variation of surface generation mechanisms in ultra-precision machining due to relative tool sharpness (RTS) and material properties, Int. J. Mach. Tool Manuf. 115 (2017) 15–28, https://doi.org/10.1016/j.ijmachtools.2016.11.003.

[29] M. Azizur Rahman, M. Rahman, A. Senthil Kumar, Influence of relative tool sharpness (RTS) on different ultra-precision machining regimes of Mg alloy, Int. J. Adv. Manuf. Technol. 96 (2018) 3545–3563, https://doi.org/10.1007/s00170-018-1599-4.

[30] S.N. Ameli Kalkhoran, M. Vahdati, J. Yan, Molecular dynamics investigation of nanometric cutting of single-crystal silicon using a blunt tool, JOM 71 (12) (2019) 4296–4304, https://doi.org/10.1007/s11837-019-03671-w.

[31] S. Plimpton, Fast parallel algorithms for short-range molecular dynamics, J. Comput. Phys. 117 (1995) 1–19, https://doi.org/10.1006/jcph.1995.1039.

[32] S.N. Ameli Kalkhoran, M. Vahdati, J. Yan, Investigation on the effect of workpiece dimension in nanometric machining of monocrystalline silicon by molecular dynamics simulation, Journal of Mechanical Engineering- University of Tabriz (2019) (in Persian), In press.

[33] S.Z. Chavoshi, S. Goel, X. Luo, Influence of temperature on the anisotropic cutting behaviour of single crystal silicon: a molecular dynamics simulation investigation, J. Manuf. Process. 23 (2016) 201–210, https://doi.org/10.1016/j.jmapro.2016.06.009.

[34] P. Zhu, Y. Hu, T. Ma, H. Wang, Study of AFM-based nanometric cutting process using molecular dynamics, Appl. Surf. Sci. 256 (2010) 7160–7165, https://doi.org/10.1016/j.apsusc.2010.05.044.

[35] J. Li, Q. Fang, L. Zhang, Y. Liu, Subsurface damage mechanism of high speed grinding process in single crystal silicon revealed by atomistic simulations, Appl. Surf. Sci. 324 (2015) 464–474, https://doi.org/10.1016/j.apsusc.2014.10.149.

[36] Y. Liu, B. Li, L. Kong, A molecular dynamics investigation into nanoscale scratching mechanism of polycrystalline silicon carbide, Comput. Mater. Sci. 148 (2018) 76–86, https://doi.org/10.1016/j.commatsci.2018.02.038.

[37] J. Li, Q. Fang, L. Zhang, Y. Liu, The effect of rough surface on nanoscale high speed grinding by a molecular dynamics simulation, Comput. Mater. Sci. 98 (2015) 252–262, https://doi.org/10.1016/j.commatsci.2014.10.069.

[38] J. Wang, X. Zhang, F. Fang, R. Chen, A numerical study on the material removal and phase transformation in the nanometric cutting of silicon, Appl. Surf. Sci. 455 (2018) 608–615, https://doi.org/10.1016/j.apsusc.2018.05.091.

[39] J. Tersoff, Empirical interatomic potential for silicon with improved elastic properties, Phys. Rev. B. 38 (1988) 9902–9905.

[40] J. Tersoff, New empirical approach for the structure and energy of covalent systems, Phys. Rev. B. 37 (1988) 6991–7000.

[41] J. Tersoff, Modeling solid-state chemistry: interatomic potentials for multicomponent systems, Phys. Rev. B. 39 (1989) 5566–5568, https://doi.org/10.1103/PhysRevB.39.5566.

[42] A. Stukowski, Visualization and analysis of atomistic simulation data with OVITO-the Open Visualization Tool, Model. Simul. Mater. Sci. Eng. 18 (2010), https://doi.org/10.1088/0965-0393/18/1/015012.

[43] H. Su, Q. Tang, Chip formation dependence of machining velocities in nano-scale by molecular dynamics simulations, Sci. China Technol. Sci. 57 (2014) 2426–2433, https://doi.org/10.1007/s11431-014-5708-9.

[44] H. Dai, G. Chen, S. Li, Q. Fang, B. Hu, Influence of laser nanostructured diamond tools on the cutting behavior of silicon by molecular dynamics simulation, RSC Adv. 7 (2017) 15596–15612, https://doi.org/10.1039/C6RA27070K.

[45] S. Goel, X. Luo, R.L. Reuben, W. Bin Rashid, Replacing diamond cutting tools with CBN for efficient nanometric cutting of silicon, Mater. Lett. 68 (2012) 507–509, https://doi.org/10.1016/j.matlet.2011.11.028.

[46] J.D. Honeycutt, H.C. Andersen, Molecular dynamics study of melting and freezing of small Lennard-Jones clusters, J. Phys. Chem. 91 (1987) 4950–4963, https://doi.org/10.1021/j100303a014.

[47] S.N. Ameli Kalkhoran, M. Vahdati, J. Yan, Investigation of ultra-precision machining using molecular dynamics simulation and experiments on single crystal silicon, Amirkabir Journal of Mechanical Engineering (2019), https://doi.org/10.22060/mej.2019.14847.6007. In press.

[48] A. Kailer, Y.G. Gogotsi, K.G. Nickel, Phase transformations of silicon caused by contact loading, J. Appl. Phys. 81 (1997) 3057–3063, https://doi.org/10.1063/1.364340.

[49] P.A. Romero, G. Anciaux, A. Molinari, J.F. Molinari, Friction at the tool–chip interface during orthogonal nanometric machining, Model. Simul. Mater. Sci. Eng. 20 (2012), 055007, https://doi.org/10.1088/0965-0393/20/5/055007.

[50] C. Ji, J. Shi, Y. Wang, Z. Liu, A numeric investigation of friction behaviors along tool/chip interface in nanometric machining of a single crystal copper structure, Int. J. Adv. Manuf. Technol. 68 (2013) 365–374, https://doi.org/10.1007/s00170-013-4734-2.

[51] D. Tao, X. Gao, H. Lu, Z. Liu, Y. Li, H. Tong, N. Pesika, Y. Meng, Y. Tian, Controllable anisotropic dry adhesion in vacuum: gecko inspired wedged surface fabricated with ultraprecision diamond cutting, Adv. Funct. Mater. 27 (2017), https://doi.org/10.1002/adfm.201606576, 1606576.

[52] G. Schnurbusch, E. Brinksmeier, O. Riemer, Influence of cutting speed on subsurface damage morphology and distribution in ground fused silica, Inventions 2 (2017) 15, https://doi.org/10.3390/inventions2030015.

[53] B.N.J. Persson, Sliding friction, Surf. Sci. Rep. 33 (1999) 83–119, https://doi.org/10.1016/S0167-5729(98)00009-0.

[54] M. Mukaida, J. Yan, Ductile machining of single-crystal silicon for microlens arrays by ultraprecision diamond turning using a slow tool servo, Int. J. Mach. Tool Manuf. 115 (2017) 2–14, https://doi.org/10.1016/j.ijmachtools.2016.11.004.

[55] A.M. Kovalchenko, Y.V. Milman, On the cracks self-healing mechanism at ductile mode cutting of silicon, Tribol. Int. 80 (2014) 166–171, https://doi.org/10.1016/j.triboint.2014.07.003.

[56] F.Z. Fang, G.X. Zhang, An experimental study of edge radius effect on cutting single crystal silicon, Int. J. Adv. Manuf. Technol. 22 (2003) 703–707, https://doi.org/10.1007/s00170-003-1593-2.

[57] Y. Mizumoto, H. Kangawa, H. Itobe, T. Tanabe, Y. Kakinuma, Influence of crystal anisotropy on subsurface damage in ultra-precision cylindrical turning of CaF2, Precis. Eng. 49 (2017) 104–114, https://doi.org/10.1016/j.precisioneng.2017.01.017.

[58] S. Goel, X. Luo, A. Agrawal, R.L. Reuben, Diamond machining of silicon: a review of advances in molecular dynamics simulation, Int. J. Mach. Tool Manuf. 88 (2015) 131–164, https://doi.org/10.1016/j.ijmachtools.2014.09.013.

[59] S.J. Zhang, S. To, S.J. Wang, Z.W. Zhu, A review of surface roughness generation in ultra-precision machining, Int. J. Mach. Tool Manuf. 91 (2015) 76–95, https://doi.org/10.1016/j.ijmachtools.2015.02.001.

[60] S.N. Ameli Kalkhoran, M. Vahdati, The effect of interatomic potential function on nanometric machining of single crystal silicon, J. Appl. Comput. Sci. Mech. 30 (2) (2019) 17–32, https://doi.org/10.22067/fum-mech.v30i2.71972.